(8) Ober, R.; Paz, L.; Taupin, C.; Pincus, P.; Boileau, S. *Macromolecules* **1983**, *16*, 50.
(9) Di Meglio, J. M.; Ober, R.; Paz, L.; Taupin, C.; Pincus, P.; Boileau, S. *J. Phys. (Les Ulis, Fr.)* **1983**, *44*, 1035.
(10) Israelachvili, J. N.; Tandon, R. K.; White, L. R. *Nature (London)* **1979**, *277*, 120. Klein, J. *Nature (London)* **1980**, *288*, 248.
(11) Israelachvili, J. N.; Tirrel, M.; Klein, J.; Almog, Y. *Macromolecules* **1984**, *17*, 205. Klein, J.; Almog, Y. *J. Colloid Interface Sci.* **1985**, *106*, 33.
(12) Poser, C. I.; Sanchez, I. C. *Macromolecules* **1981**, *14*, 361.
(13) Leibler, L. *Macromolecules* **1982**, *15*, 1283.
(14) Hadziioannou, G.; Patel, S.; Granick, S.; Tirrell, M. *J. Am. Chem. Soc.* **1986**, *108*, 2869.
(15) Granick, S.; Patel, S.; Tirrell, M. *J. Chem. Phys.* **1986**, *85*, 5370.
(16) Fredrickson, G. H. *Macromolecules* **1987**, *20*, 2535.
(17) Marques, C. M.; Joanny, J. F.; Leibler, L., preprint, 1987.
(18) Moore, M. A. *J. Phys. A: Math. Gen.* **1977**, *10*, 305.
(19) The relation between the effective excluded volume parameters w_{AA}, w_{BB}, and w_{AB} and the Flory parameters is as follows: Let Φ_A, Φ_B, and Φ_S be the volume fractions of polymer A, polymer B, and solvent, respectively. The Flory–Huggins free-energy form $F = F_{mix} + F_{int}$, where (in the long chain limit) $F_{mix} = T\Phi_S \ln \Phi_S$ and

$$F_{int}/T = \tfrac{1}{2}\sum_{ij}\chi_{ij}^{dir}\Phi_i\Phi_j$$

Expanding to quadratic order in Φ_A and Φ_B (and using $\sum_i\Phi_i = 1$), we obtain

$$F/T = \tfrac{1}{2}(\Phi_A + \Phi_B)^2 - \sum_{ij}\chi_{ij}\Phi_i\Phi_j$$

where the sum is over species A and B only. The resulting Flory-type parameters obey

$$\chi_{AA} = \chi_{AS}^{dir} - (\chi_{AA}^{dir} + \chi_{SS}^{dir})/2$$

$$\chi_{BB} = \chi_{BS}^{dir} - (\chi_{BB}^{dir} + \chi_{SS}^{dir})/2$$

$$\chi_{AB} = (\chi_{AS}^{dir} + \chi_{BS}^{dir} - \chi_{AB}^{dir} - \chi_{SS}^{dir})/2$$

On the other hand, in terms of the excluded volume parameters, F is written as

$$F/T = \tfrac{1}{2}\sum_{ij}w_{ij}\Phi_i\Phi_j$$

Hence the excluded volume parameters are related to the Flory χ parameters as follows:

$$w_{AA} = 1 - 2\chi_{AS}$$

$$w_{BB} = 1 - 2\chi_{BS}$$

$$w_{AB} = 1 - 2\chi_{AB}$$

(20) Note that the unit of length ξ_A does depend on these parameters. On the other hand, the surface potential experienced by the polymer is independent of the bulk parameters. Therefore, we introduce the dimensionless surface parameters $\kappa_A^0 = \xi_A^0\kappa_A$ and $\kappa_B^0 = \xi_A^0\kappa_B$; we ask that the logarithmic derivative of f_A and f_B with respect to x be equal to $(\xi_A/\xi_A^0)\kappa_A^0$ and $(\xi_A/\xi_A^0)\kappa_B^0$, respectively.
(21) Under the assumption that the free energy is dominated by two-body repulsions, the bulk free energy per unit volume for the mixture is

$$f_{mix} = (w_{AA}c_A^2 + w_{BB}c_B^2 + 2w_{AB}c_Ac_B)/2$$

while for a phase-separated state

$$f_{ps} = (w_{AA}c_A^2 + w_{BB}c_B^2 + 2(w_{AA}w_{BB})^{1/2}c_Ac_B)/2$$

from which (15) follows immediately.
(22) We are indebted to Prof. Daniel W. Hone for illuminating comments on this point.

Interphase Composition Profile in SB/SBS Block Copolymers, Measured with Electron Microscopy, and Microstructural Implications

Richard J. Spontak and Michael C. Williams*

Center for Advanced Materials, Lawrence Berkeley Laboratory, and Department of Chemical Engineering, University of California, Berkeley, California 94720-9989

David A. Agard

Department of Biochemistry and Biophysics, University of California, San Francisco, California 94143-0448. *Received May 4, 1987; Revised Manuscript Received September 4, 1987*

ABSTRACT: The behavior of microphase-separated block copolymers has major contributions from the mixed interphase existing between the two homogeneous phases. However, relatively little has been known about the interphase itself and, in particular, its composition profile has never been measured directly. Here, we have used quantitative transmission electron microscopy to acquire the shape of the volume-fraction composition profile across this interphase. Measurements were made on four styrene (S)/butadiene (B) block copolymers having structure SBS (three) and SB (one), with molecular weights 1.0–2.3 × 10^5 g/mol and overall volume compositions of 0.24–0.38 styrene. Results, averaged over the four samples, depict an asymmetric interphase profile, being rich in styrene (54 vol %) in agreement with new differential scanning calorimetry data and with dynamic mechanical testing studies of others. This profile is then used in an equilibrium thermodynamic theory (which extends earlier work by adding an enthalpic "Debye" term that accounts for molecular interactions beyond nearest neighbors) to predict various microstructural and thermal properties of the bulk polymer. Excellent agreement with reported data is obtained for the predicted interphase thickness and interphase volume fraction and for predictions of the repeat distance for lamellar SB copolymers.

Introduction

Block copolymers are known to undergo microphase separation under certain conditions (normally encountered in practice) of composition, molecular weight, temperature, and molecular architecture. The result of this microphase separation is the formation of either a cocontinuous composite of lamellar elements or a dispersed phase of domains distributed in a continuous matrix (Figure 1). Since these microphase-separated block copolymers exhibit thermal and mechanical properties unlike those of either homopolymer or a random copolymer of similar composition,

* To whom correspondence should be addressed.

0024-9297/88/2221-1377$01.50/0 © 1988 American Chemical Society

Table I
Macroscopic Properties of the SB/SBS Block Copolymers Used in This Study[a]

sample[b]	architecture	morphology	$\bar{M}_n \times 10^{-3}$, g/mol	$\bar{M}_w/\bar{M}_n$	$\bar{M}_S \times 10^{-3}$, g/mol	w_S	ϕ_S
F411	SBS	CYL	115.0	2.00	34.5	0.30	0.28
F414	SBS	LAM	87.7	1.71	30.0	0.40	0.38
F416	SBS	CYL	84.8	1.65	21.0	0.30	0.28
F1205	SB	CYL/LAM	71.4	1.40	25.0	0.25	0.24

[a] All bulk properties have been characterized by Cosden Oil and Chemical Co. [b] F is an abbreviation for Finaprene.

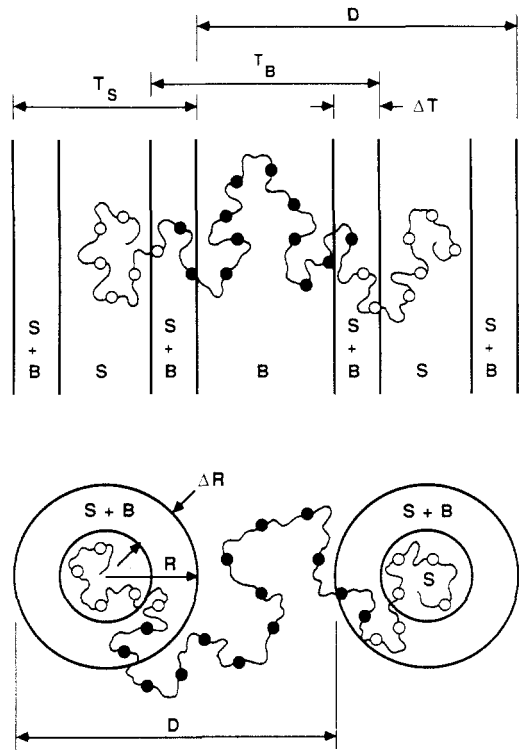

Figure 1. Schematic representation of lamellar (top) and spherical/cylindrical (bottom) microstructures resulting from microphase separation in block copolymers. In this case, S represents styrene and B butadiene, and the triblock case is shown explicitly.

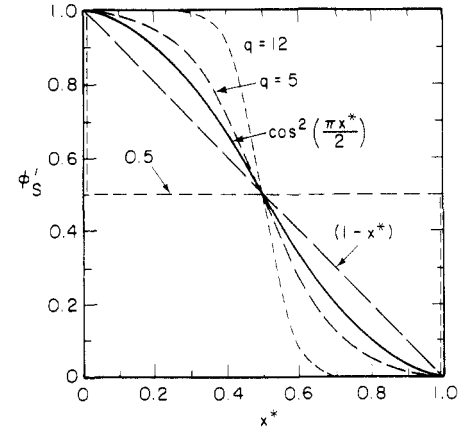

Figure 2. Symmetric interphase composition profiles used in the sensitivity analysis of Henderson and Williams.[14] The analytical functions are as follows: step ($\phi'_S = 0.5$), linear ($\phi'_S = 1 - x^*$), sinusoidal ($\phi'_S = \cos^2(\pi x^*/2)$), and hyperbolic tangent ($\phi'_S = 0.5 - 0.5 \tanh [q(x^* - 0.5)]$, with $q = 5$ or 12).

many investigators have sought to establish and understand the relationship between these bulk properties and the microstructures. One conclusion reached in these studies has been that the interphase, the region that remains partially and inhomogeneously mixed between the adjacent homogeneous phases, is a major factor in determining many bulk properties and moreover is solely responsible for a number of unique phenomena (e.g., the plastic-to-rubber transition upon stretching[1] and the yield stress in melts[2]). Across this interphase, whose thickness is designated in Figure 1 as ΔR in spherical/cylindrical and as ΔT in lamellar microstructures, the local composition goes from primarily pure S (styrene) to pure B (butadiene). Minimization of the free energy of the entire copolymer system[3-7] causes a large-fraction interphase to be favored, making its detailed description important.

Both the extent of the interphase and its composition profile, however, have not always been recognized as essential features of these complex microcomposites. For instance, the equilibrium thermodynamic theories proposed by Meier[8] and by Krause[9] initially assumed the existence of a sharp interphase. The earliest theory developed by Leary and Williams,[5,6] however, proposed a finite interphase with the composition profile handled, for simplicity, as a constant equal to the average (0.5) of the end points (0,1). Developments in the theories of Helfand,[10-12] Meier,[13] and Henderson and Williams[14] eventually incorporated more realistic symmetric composition profiles. Henderson and Williams[14] analyzed the effects of profile shape variation (see Figure 2) on the microstructural and thermal properties predicted by their theory. The five profiles they chose were expressed in terms of $\phi'_S(x^*)$, the local volume fraction of S, where

$$x^* = \hat{x}/I \tag{1}$$

with $\hat{x}$ the position in the interphase measured from the S-phase side and I the interphase thickness (ΔR or ΔT). Recent advances in experimental techniques—for example, small-angle X-ray scattering (SAXS),[15-19] small-angle neutron scattering (SANS),[20-25] differential scanning calorimetry (DSC),[26] and dynamic mechanical testing (DMT)[1,27-31]—have complemented the theoretical studies by providing more data on interphase thicknesses and compositions. As reviewed recently,[32] the preponderance of evidence (all indirect) supports the existence of asymmetric interphase compositions in general. Some DMT and DSC studies, for example, indirectly revealed that the interphases were rich in the hard-segment component; that is, $\phi'_S(x^*)$ was asymmetric. [Similar asymmetries have been reported by Wu et al.[33] for the interphases existing in incompatible poly(methyl methacrylate) and poly(vinylidene fluoride) blends.] Prompted by this evidence, Henderson and Williams[34] incorporated asymmetric composition profiles into their theory and studied the resulting effects on predicted microstructural and bulk properties.

However, the actual composition profiles across the interphase in block copolymers have heretofore not been directly ascertained. In the present work, we employ quantitative transmission electron microscopy to obtain these profiles and then use them in the Henderson–Williams theory to predict microstructural properties.

Experimental Section

Four block copolymer samples of styrene–butadiene character were provided by Cosden Oil and Chemical Co. (Deer Park, TX 77536) and are characterized in Table I. In order to use low-

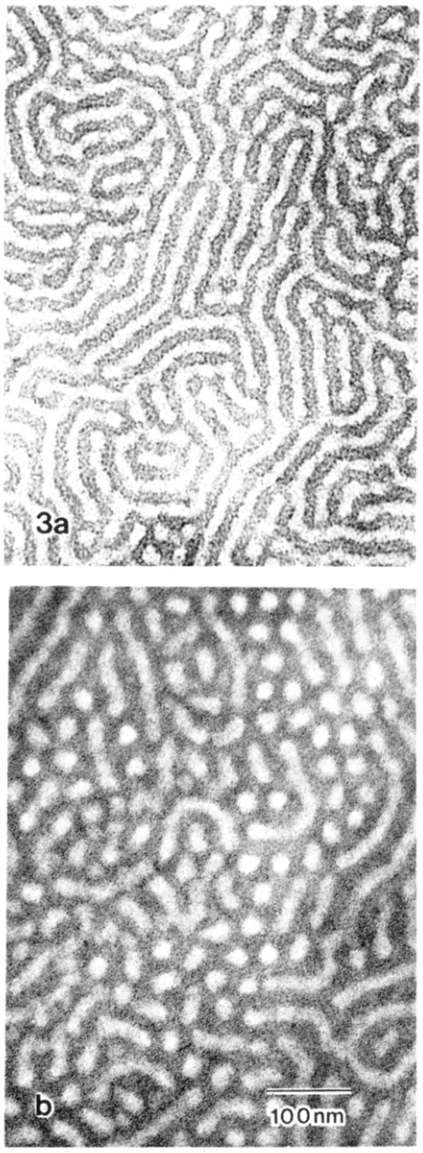

Figure 3. Typical electron micrographs taken with a JEOL JEM 100CX of samples (a) F414, showing lamellar morphology, and (b) F1205, with mixed cylindrical and lamellar domains. The B blocks, stained with OsO_4 to enhance contrast, constitute the dark matrices.

voltage TEM, ultrathin polymeric sections or films less than 1000 Å thick must be obtained. Even more constraining was the goal of gaining information from a region (the interphase) only 20–30 Å in width; for this, the film thickness had to be less than about 400 Å.[35] In this study, we utilized a new direct-casting technique (presented elsewhere[36]) to produce ultrathin films from solutions in toluene. These films were 300–400 Å in thickness as determined from a three-dimensional reconstruction of the film.[37] The sample films were stained at room temperature with the vapor of a 1% osmium tetraoxide aqueous solution for 85 min to enhance contrast between phases. These staining conditions were chosen to be consistent with those found[19] to produce a stain intensity proportional to the concentration of double bonds in the rubbery phase. Exposure of a polystyrene film to OsO_4 vapors under these conditions produced no detectable staining. Electron micrographs were obtained by using a JEOL JEM 100CX (JEOL Ltd., Peabody, MA 01960) at various magnifications from 33000× to 100000× at an accelerating voltage of 80 kV.

Image Analysis

Electron micrographs, examples of which are shown in Figure 3, were digitized by using an Eikonixscan Model 785 image digitizer (Eikonix Corp., Bedford, MA 01730) and a Perkin-Elmer (Garden Grove, CA 92641) PDS microdensitometer set at a 17-μm spot size. The images, measuring 512 pixels × 512 pixels, were then utilized in studying $\phi'_S(x^*)$. This analysis was based on evidence[19,38] that the dark regions of the image corresponded to the OsO_4-stained double bonds of the butadiene and the light regions corresponded to styrene.

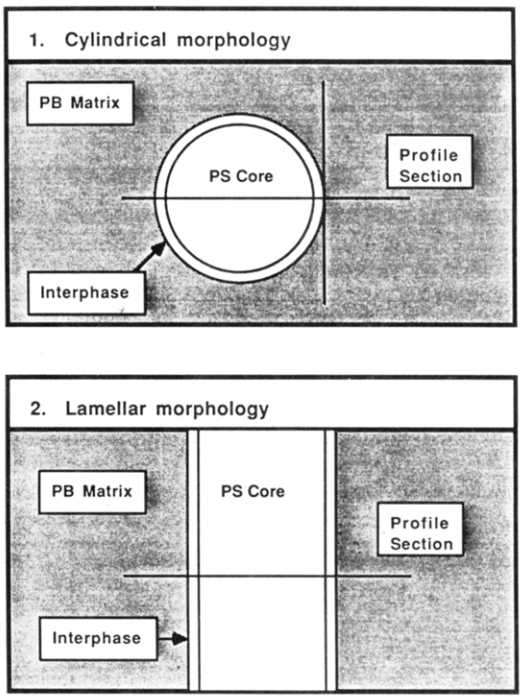

Figure 4. Locations used for obtaining optical-density profiles across the interphase regions of (1) cylindrical and (2) lamellar microstructures. Note that the profile sections are taken radially and perpendicularly to the interphases of the cylinders and lamellae, respectively.

The analysis began by selection of domain images that corresponded to the idealizations shown in Figure 4 —i.e., circular cylinders and lamellae oriented normal to the film surface. This avoided the necessity of making geometrical corrections due to distortions and imperfections (e.g., tilt) in the image of the domain being studied. Domains extended through the thickness of the ultrathin film, with the polystyrene core exposed at the surface and not shielded by any polybutadiene layer. All these geometrical features of the domains were confirmed by our extended study[37] of the microstructure with tomagraphic techniques that produced a three-dimensional "reconstruction" of the film. The phenomenon of domains extending entirely through such films has been reported by investigators[39,40] using X-ray photoelectron spectroscopy (XPS) to study surfaces of styrene–(ethylene oxide) block copolymers.

After selection of suitable domain subjects, the analysis proceeded by obtaining the optical-density profiles across the domains at specific locations, as diagrammed in Figure 4. In the case of the cylindrical morphology (e.g., portions of Figure 3b), the profile sections were the diameters of the two-dimensional circular cross-sections of the cylinders (see Figures 4 and 5). Four profiles were obtained from *each* domain studied, and upon comparison of these profiles (some of which were at 90° to each other), little variation was detected, further substantiating the absence of domain tilt. In the case of the lamellae (e.g., Figure 3a), the profile sections were obtained in a fashion similar to that described by Annighofer and Gronski[19] (see Figure 4). After optical-density profiles were acquired for each of the microstructures in the four samples, the noise level was reduced by averaging the selected profile sections (1

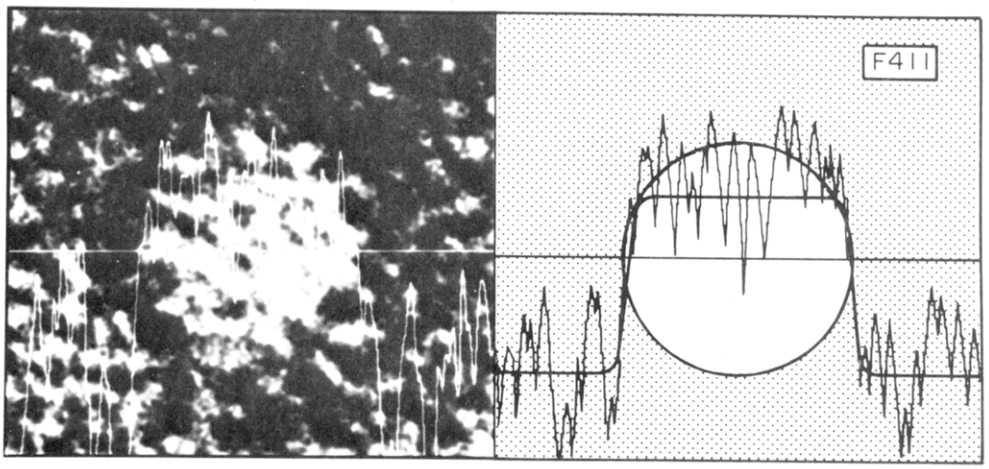

Figure 5. Image-enhanced electron micrograph (left) from a sample of polymer F411, showing an optical-density trace across a cylindrical S domain. The corresponding average and its smoothed profile are portrayed to the right.

pixel in width) with the two adjacent profile sections (each also being 1 pixel in width). This method of image enhancement causes some smearing of the images[41] but keeps intact the optical-density variation from light region to dark region.

Polymer composition across the interphase was obtained from the optical density by the following procedure. First, electron absorption in the sample is characterized as described by Grum and Becherer:[42]

$$\Phi_f(x,y,z) = \Phi_0 e^{-P_z(x,y)z} \tag{2}$$

where Φ_0 and Φ_f are the intensities of the electron beam before and after penetrating the TEM film at location (x,y) on the image, $P_z(x,y)$ is the linear absorption coefficient at (x,y), and z is the depth of penetration. Since, however, we are interested only in the flux exiting the film ($z = t$) and the thickness of each TEM specimen examined is constant,[37] t can be incorporated into P_z and $\Phi_f = \Phi_f(x,y)$ only. Assuming the film response to be linear with regard to the electron dose, we can now define the optical density, $\rho^0(x,y)$, as

$$\rho^0(x,y) = \frac{\Phi_f(x,y)}{\Phi_0} \tag{3}$$

To account for $\rho^0(x,y)$ variations in the micrographs used (due, for example, to differing exposure times), the optical density of each micrograph is scaled with respect to that of a reference micrograph. If λ is the scaling parameter, then

$$\lambda_j = [\sum_{i=1}^{n}\sum_{m=1}^{n} \rho^0(x_i,y_m)]_{ref} / [\sum_{i=1}^{n}\sum_{m=1}^{n} \rho^0(x_i,y_m)]_j \tag{4}$$

where $\rho^0(x_i,y_m)$ is a single optical-density element of the image matrix ρ^0, n (=512) is the size of the matrix, and the subscripts j and ref denote the jth and reference micrographs, respectively. Once determined, λ_j can be used to scale each micrograph according to

$$\tilde{\rho}_j^{\,0} = \lambda_j \rho_j^{\,0} \tag{5}$$

Here $\rho_j^{\,0}$ is the matrix of optical densities for the jth micrograph, and the $\tilde{\rho}_j^{\,0}$ refers to the scaled matrix. By substituting these scaled densities (eq 5) into eq 2 and 3, we obtain

$$P_z(x,y) = -\ln \tilde{\rho}^0(x,y) \tag{6}$$

Finally, the path of least electron absorption (P_z^{min}) corresponds to the pure-styrene core and the greatest absorption (P_z^{max}) to the pure-butadiene matrix, so these two measured parameters are used to normalize data. From this, the local interphase styrene weight fraction (w'_S) along the axis of the profile section ($\hat{x}$) is

$$w'_S(\hat{x}) = \frac{P_z(\hat{x}) - P_z^{max}(\hat{x})}{P_z^{min}(\hat{x}) - P_z^{max}(\hat{x})} \tag{7}$$

This normalization, in addition to the section averaging, provides us with the interphase composition profile as a function of interphase distance. Thus, the desired local volume fraction across the interphase is

$$\phi'_S(\hat{x}) = \frac{w'_S(\hat{x})/\rho_S}{w'_S(\hat{x})/\rho_S + w'_B(\hat{x})/\rho_B} \tag{8}$$

Here, ρ_S and ρ_B are the mass densities of styrene (1.05 g/cm^3) and butadiene (0.97 g/cm^3), respectively.

Once converted to weight fractions, these profiles (expressed in terms of x^*) were smoothed by using a cubic-spline function,[43] and the profiles for each sample microstructure were averaged. Since the profiles were averaged over several micrographs (at least 10 for each copolymer), which varied in magnification and overall optical density, any remaining artifacts due to nonlinearities in the response of the photographic-film emulsion to the electron exposure were completely eliminated. The weight-fraction composition profiles were then converted to volume-fraction profiles by eq 8. The results of this analysis are presented in Figure 6 for each of the four copolymer samples. In each case, the local composition profile is asymmetric in favor of the interphase being rich in styrene. The total styrene volumetric content within the interphase is

$$\overline{\phi'_S} = 1 - \overline{\phi'_B} = \int_0^1 \phi'_S(x^*)\, dx^* \tag{9}$$

Values of $\overline{\phi'_S}$ for all copolymer samples are tabulated in Table II.

Comparison can be made between these TEM-obtained values of $\overline{\phi'_S}$ and those inferred from glass transition measurements (Figure 7) obtained with a Mettler FP84 DSC (Mettler Instrument Corp., Highstown, NJ 08520). The inference requires that the measured value (designated T'_g) represents T_g of a hypothetical uniform S/B blend at a composition equal to $\overline{\phi'_S}$. Following the arguments of Henderson and Williams,[32] we first estimate the $T'_g(w'_S)$ function in two ways: the linear weighting rule for T'_g,

$$T'_g = \overline{w'_S} T_g^S + \overline{w'_B} T_g^B \tag{10}$$

and the inverted, or Fox, rule

$$1/T'_g = \overline{w'_S}/T_g^S + \overline{w'_B}/T_g^B \tag{11}$$

Table II
Microstructural and Related Properties of the SB/SBS Block Copolymer Used in This Study

			profile[c]		linear[d]		Fox[e]		
sample	T_g,[a] K	T_g^S,[b] K	w'_S	$\overline{\phi'_S}$	$\overline{w'_S}$	$\overline{\phi'_S}$	$\overline{w'_S}$	$\overline{\phi'_S}$	D,[f] Å
F411	338.2	367.4	0.57	0.55	0.83	0.82	0.90	0.90	422 ± 21
F414	342.0	369.8	0.56	0.54	0.84	0.83	0.91	0.90	293 ± 18
F416	339.1	368.4	0.54	0.52	0.83	0.82	0.90	0.90	398 ± 30
F1205	340.4	365.2	0.57	0.55	0.86	0.85	0.92	0.91	393 ± 18

[a] Measured by DSC using a Mettler FP84 DSC at a heating rate of 5 deg/min. [b] Calculated from $T_g^S = T_g^\infty - k/\bar{M}_S$, where $k = 2 \times 10^5$ for $\bar{M}_S > 10^4$ g/mol and $T_g^\infty = 373.15$ K.[32] [c] Determined from eq 9. [d] Determined by solving eq 10 for $\overline{w_S'}$ and using $T_g^B = 193.15$ K. [e] Computed by rearranging eq 11 and using T_g^B as above. [f] Given as an average, with a standard deviation.

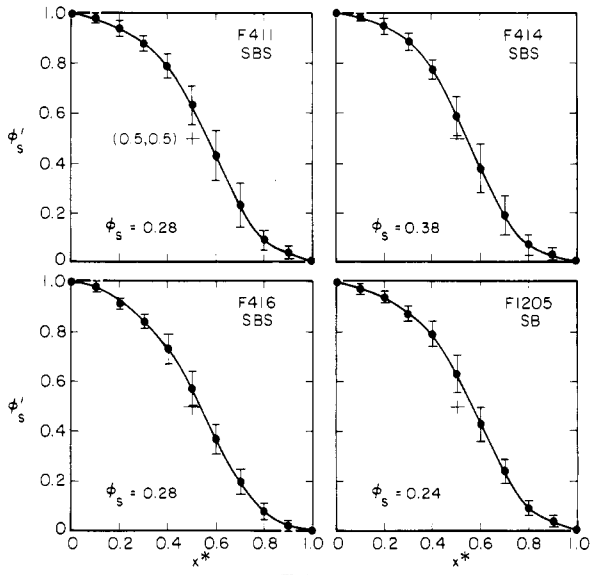

Figure 6. Interphase composition profiles (volume fraction of styrene as a function of interphase position) obtained for four polymer grades from the digitized electron micrographs. In all cases, the average profile passes above the (0.5,0.5) point, and the overall interphase composition, given as the area under each curve, yields $\overline{\phi'_S} > 0.5$.

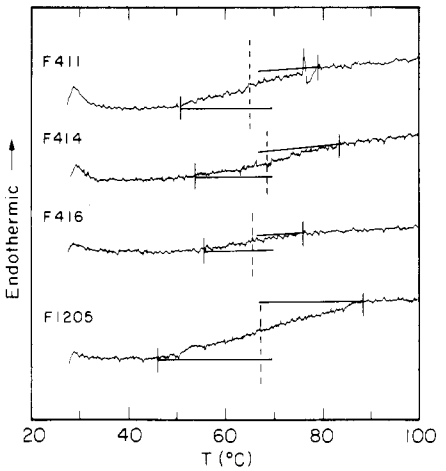

Figure 7. Differential scanning calorimetry traces for the polymer samples (a) F411, (b) F414, (c) F416, and (d) F1205 obtained with a Mettler FP84 DSC and showing the locations of T'_g (dashed lines). In each case, the heating rate was 5 deg/min.

Then, $\overline{w'_S}$ (and $\overline{\phi'_S}$) can be inferred from the DSC data. Table II shows that the linear rule produces compositions more closely in agreement with those of the TEM profiles, although both rules overestimate the styrene content significantly. The T'_g analysis tends to set the average styrene composition at either 83 vol % (linear) or 90 vol % (Fox), while the profiles yield an averge of 54 vol %. Clearly, the DSC data cannot be interpreted quantitatively in the manner invoked here (the interphase is not a homogeneous region), but the trends of styrene-rich interphases are still evident. Both TEM and DSC data provide direct evidence that the interphase feeds preferentially on the S block to yield the observed T'_g shift.

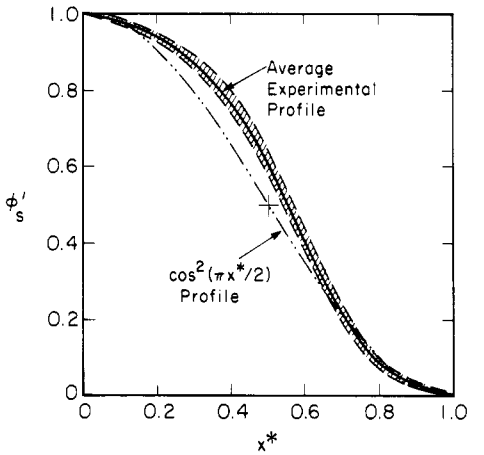

Figure 8. Average experimental interphase composition profile determined by superimposing the four average profiles found in Figure 6. As seen from the shaded region, little deviation occurs between the upper and lower limits of variation. The symmetric $\cos^2(\pi x^*/2)$ profile is also presented to demonstrate the asymmetry in the experimental profile.

If all four experimental profiles are superimposed (Figure 8), it is clear that little variation is shown. In Figure 8, an average profile (arithmetic average of the four measured curves) is presented along with the symmetric $\cos^2(\pi x^*/2)$ function. The reason for choosing the $\cos^2$ function for comparison is that Henderson and Williams[14] demonstrated good agreement between theory incorporating this $\phi'_S(x^*)$ and SAXS data[17] on total interphase thickness. In addition, the rheological studies of Kraus and Rollmann[28] indicated that, in order to satisfy the $G'(T)$ and $G''(T)$ data on their SBS and SIS block copolymers, the interphase composition profile must be asymmetric but must not deviate very much from a sinusoidal function such as the one above.

It is worthwhile to assess the presence of the OsO_4 stain molecule as a possible source of artifacts here. At worst, it would contribute extra volume to regions where PB chains exist and thus swell those regions in proportion to the local PB concentration. This would mean, in the interphase, that the $\phi'_S(x^*)$ profiles would be biased in the direction of butadiene richness—i.e., the finding that the profiles are styrene-rich would be an understatement of exactly how rich they really are (in the absence of OsO_4).

While this possibility cannot be completely dismissed, we do not believe it is likely or important. We believe that the OsO_4 molecule occupies primarily the free volume of the rubbery regions, not stretching those regions significantly. There are three observations that support this contention. First, a study of time-dependent staining[19]

showed that the micrographs over a period of 1–100 min maintained a constant ratio of dark to light areas, indicating that increasing OsO_4 uptake was not contributing measurably to the rubber volume. Second, our own work[38] demonstrated that the dark/light area ratio in micrographs corresponds very closely to the known PB/PS volume ratios in these copolymers; this would not be true if the PB regions were expanded by OsO_4. Third, there was no macroscopic evidence that these samples or others made from the same material were swollen by the staining process.

Thermodynamic Theory

The details of this model have been presented at length elsewhere,[5,6,14,34] and therefore only a brief summary is presented here. As a system strives toward equilibrium, it tends to seek a minimum in its free energy. That is,

$$\Delta G \rightarrow \Delta G_{min} = (\Delta H - T\Delta S)_{min} \tag{12}$$

where ΔG is the difference in Gibbs free energy between the structured (i.e., microphase-separated) copolymer and its homogeneous analogue at the same conditions of temperature, composition, molecular weight, and molecular architecture.

The entropic term, ΔS, which is sensitive to molecular architecture, is the result of three contributions,

$$\Delta S = \Delta S_S + \Delta S_B + \Delta S_I \tag{13}$$

Here, ΔS_I reflects the confinement of the block junction to the interphase region, and ΔS_k (k = S or B) is the change in entropy, with respect to the homogeneous analogue, that occurs by forcing the kth block to reside in T_k, where T_k is the demixed k region and its two adjacent interphases (see Figure 1). Williams and co-workers[6,14] have shown that

$$\Delta S_I^{di} = R \ln (f) \tag{14a}$$

$$\Delta S_I^{tri} = R \ln (2f - f^2) \tag{14b}$$

where R is the gas constant and f represents the fraction of material found within the interphase; superscripts di and tri refer to diblock and triblock architectures, respectively. Expressions for f can be derived from material balances and depend on the morphology:

cylindrical domains of styrene

$$f = \frac{[1 - (1 - \beta)^2]\phi_S}{(1 - \beta)^2 + \overline{\phi'_S}[1 - (1 - \beta)^2]} \tag{15a}$$

lamellar domains

$$f = \frac{2\beta\phi_S}{1 - 2\beta\overline{\phi'_B}} \tag{15b}$$

Here, β is the dimensionless interphase thickness defined as

$$\beta \equiv I/L \tag{16}$$

where L is the characteristic dimension of the microstructural element (R or T_S in Figure 1).

The ΔS_k terms are derived from random-flight chain statistics and probability functions discussed elsewhere.[6,14] Here, the molecular architecture must again be considered. In a diblock (SB) copolymer having dispersed styrene microstructures, the S block is restricted to the domain while the rubbery B block is able to diffuse freely in the matrix. In a triblock (SBS) having similar microstructures, both ends of the chain are confined to reside in domains. In this latter architecture, the motion of the B block is limited significantly. These physical pictures, when interpreted statistically for monodisperse chains, lead directly to the functional forms

$$\Delta S_k^{di} = \Psi_k^{di}(\alpha_k, P_k) \tag{17a}$$

$$\Delta S_k^{tri} = \Psi_k^{tri}(\alpha_k, P_k) \tag{17b}$$

where Ψ_k depends on the architecture and morphology of the system and P_k is the probability function.[5,6,14] The chain expansion coefficient α_k reflects the perturbation in the end-to-end distance of the confined k block with respect to the unconfined kth homopolymer. That is,

$$\alpha_k^2 = \langle r_k^2 \rangle / \langle r_k^2 \rangle_0 \tag{18}$$

This parameter is used to account for elastic entropic contributions and is related to the dimensionless domain size

$$\Gamma \equiv T_S^2 / \langle r_S^2 \rangle \tag{19}$$

which appears explicitly in the theory.

A major complication in evaluating the theory has always existed in the enthalpic term, which assumes a regular-solution form for demixing:

$$\Delta H = -\Delta H_{mix} = -\tilde{V}(\delta_S - \delta_B)^2[\phi_S\phi_B - f\overline{\phi'_S\phi'_B}] \tag{20}$$

where $\tilde{V}$ is the total molar volume, δ_S and δ_B are the solubility parameters, and the quantity $\overline{\phi'_S\phi'_B}$ incorporates detailed information about the interphase composition:

$$\overline{\phi'_S\phi'_B} = \frac{1}{I}\int_0^I \left[\phi'_S(\hat{x})\phi'_B(\hat{x}) + \frac{t_D^2}{6}\left(\frac{d\phi'_S(\hat{x})}{d\hat{x}}\right)^2 \right] d\hat{x} \tag{21}$$

Here, t_D is the Debye molecular interaction parameter and is equal to approximately 6 Å.[44] [This corrects a typographical error in a previous publication[34] wherein the Debye term was displayed without the exponent 2 (in eq 23 of that paper).] If $\hat{x}$ is normalized according to eq 1, then eq 21 becomes

$$\overline{\phi'_S\phi'_B} = \int_0^1 \left[\phi'_S(x^*)\phi'_B(x^*) + \frac{t_D^2}{6I^2}\left(\frac{d\phi'_S(x^*)}{dx^*}\right)^2 \right] dx^* \tag{22}$$

in which $\phi'_S(x^*)$ information from Figure 6 can be used.

By varying the parameters β and Γ, a minimum is found in ΔG. If $\Delta G_{min} < 0$, then the equilibrium state is phase-separated and β_{min} and Γ_{min} correspond to this condition. From the values of β_{min} and Γ_{min}, we can directly determine the magnitudes of all microstructural properties—e.g., the interphase thickness, the core thickness, and the repeat distance (D).

Model Predictions and Discussion

We first examine the effect of the Debye term $[(t_D^2/6I^2)(d\phi'_S(x^*)/dx^*)^2]$ in eq 22 on microstructural properties; its influence is not immediately evident because of the magnifying effect of potentially steep gradients in ϕ'_S. Model calculations of ΔT were made by using the sinusoidal profile, a lamellar morphology, and the same physical parameters reported by Henderson and Williams,[14] while varying t_D from 0 to 6 Å; results are displayed in Figure 9. At 298 K, the temperature at which all predictions in this work are made, the Debye term appears simply to shift the thickness of the SBS interphase by +0.5 Å, a 2.5% increase. In the SB case, the effect is qualitatively different, varying from a 1.5 Å increase at $\phi_S = 0.35$ to almost nothing at $\phi_S = 0.65$. Since this term does affect each architecture differently, we have retained it here for the sake of completeness. Calculations hereafter will employ the experimental ϕ'_S as well as the $\cos^2$ model.

Table III
Range of Average Experimental Interphase Compositions and Corresponding Coefficients of the Expressions $\phi'_S(x^*) = \sum_{i=0}^{7} A_i(x^*)^i$

$\overline{\phi'_S}^a$	$\overline{\phi'_S\phi'_B}^b$	A_7	A_6	A_5	A_4	A_3	A_2	A_1	A_0
0.558	0.114	7.5864	−58.905	125.29	−109.78	42.903	−8.5163	0.42509	1.0000
0.524	0.111	7.5864	−44.853	83.129	−63.200	20.008	−3.6051	−0.06426	1.0000

[a] Calculated from eq 9. [b] Calculated for eq 22 with $t_D = 0$ Å. (In the case of $t_D = 6$ Å, $\overline{\phi'_S\phi'_B} = \overline{\phi'_S\phi'_B}(I)$, where I is a function of molecular weight, bulk composition, and molecular architecture.)

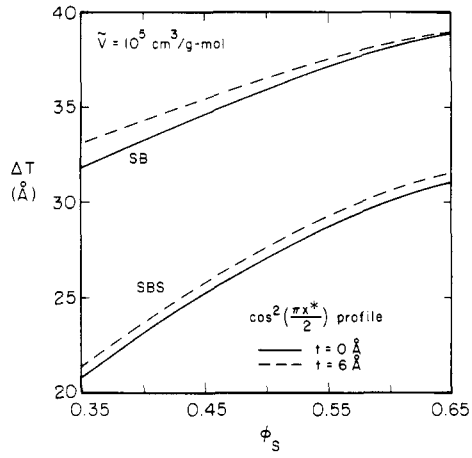

Figure 9. Influence of the Debye molecular interaction parameter on the calculated interphase thickness (ΔT) for lamellar SB/SBS copolymers. Here, $\tilde{V}$ is constant and the $\cos^2$ profile is used. The addition of the Debye term simply shifts the SBS curve upward by a constant amount (about 0.5 Å). In the SB case, the degree of the thickness increase is dependent upon the bulk composition.

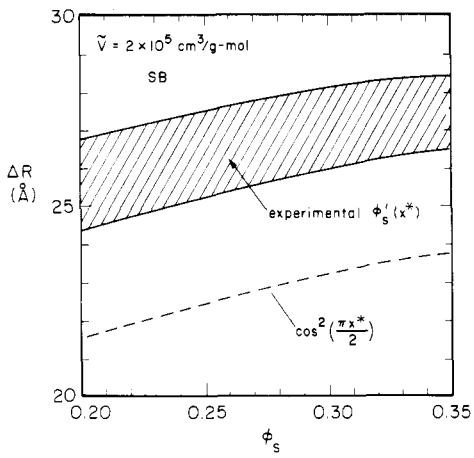

Figure 10. Interphase thickness (ΔR) as a function of bulk composition for cylindrical SB morphologies. Predictions made by incorporating the experimental interphase composition profile (shaded) exceed those made by using the $\cos^2$ function (dashed). The shaded region is explained in the text.

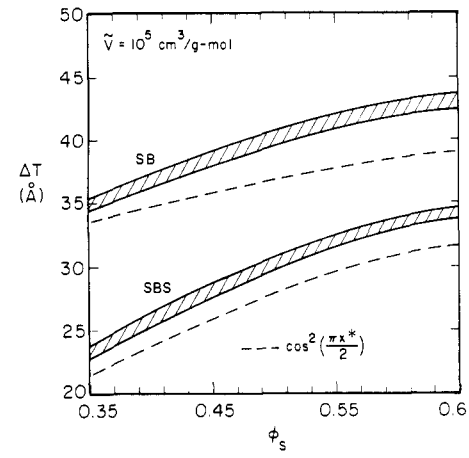

Figure 11. Interphase thickness (ΔT) predicted for lamellar SB/SBS copolymers by using the experimental $\phi'_S(x^*)$ (shaded) is wider than that predicted with the $\cos^2$ profile (dashed). For the SBS case, ΔT is translated upward by an almost constant value, but the SB case behaves differently.

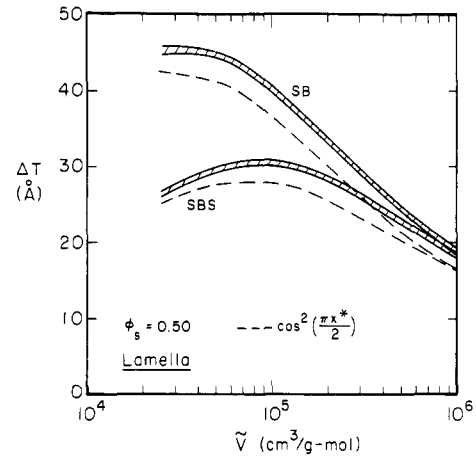

Figure 12. Interphase thickness for lamellar SB/SBS copolymers as a function of molar volume or approximate molecular weight. In each case, the thickness predicted from the experimental profile (shaded) is greater than that from the $\cos^2$ profile (dashed).

The crosshatched region of Figure 8 shows that some variation does exist in $\phi'_S(x^*)$ measured for different polymers, so both the upper and lower bounds of this region were used in many of the following calculations. Both boundary lines were fitted by a seventh-order polynomial expression, using a standard least-squares routine. The coefficients of these expressions are presented in Table III, along with the corresponding values of $\overline{\phi'_S}$ and $\overline{\phi'_S\phi'_B}$.

1. Interphase Thickness. In Figure 10, ΔR for an SB copolymer exhibiting cylindrical morphology ($0.20 \leq \phi_S \leq 0.35$) is presented as a function of bulk composition. Here, we see that ΔR predicted from the experimental $\phi'_S(x^*)$ exceeds that predicted from the sinusoidal ($\cos^2$) profile by 3.5–5.0 Å. A similar trend for lamellar morphologies ($0.35 \leq \phi_S \leq 0.65$) is noted in Figure 11, which represents SB and SBS copolymers. The triblock case using the experimental $\phi'_S(x^*)$ deviates from the case using the $\cos^2$ profile by an almost constant 1.0–2.0 Å. The diblock, however, shows greater deviation (3.5–4.5 Å at $\phi_S = 0.65$). In both Figures 10 and 11, the upper limit of the shaded regions corresponds to the upper bound of the experimental $\phi'_S(x^*)$. This means that S enrichment of the interphase is achieved by stretching the phase boundaries to allow for the extra styrene volume, which in turn reduces the volume of the homogeneous S phase.

The relationship between ΔT and $\tilde{V}$ (which approximates the total molecular weight) is depicted in Figure 12 for the case $\phi_S = 0.5$ (lamellar microstructure). Use of the experimental $\phi'_S(x^*)$ gives ΔT values which exceed the $\cos^2$ profile results by about 4.0–5.0 Å over the entire $\tilde{V}$ range (to $\tilde{V} = 10^6$). Contrary to the theory of Helfand,[4] both SB and SBS interphases exhibit a significant decrease at high

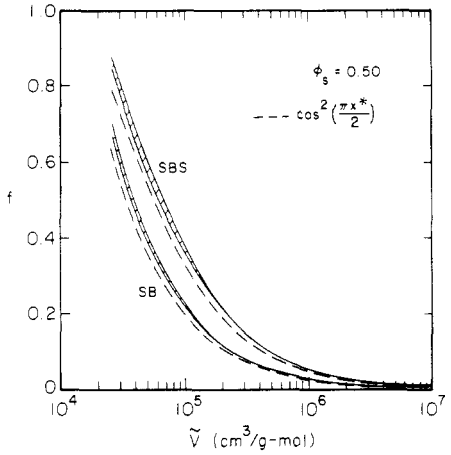

Figure 13. Fraction of material in the interphase region (f) as a function of molar volume for lamellar SB/SBS cases. For each, f is greater when predicted from the experimental profile (shaded) than from the sinusoidal profile (dashed), and the triblock has larger f than the diblock (as expected, since it has more junctions per molecule). Also, this function approaches $f = 1$ at low molecular weights, thereby indicating that no microphase separation would occur for $\tilde{V}$ below a certain value (as seen also in Figure 12).

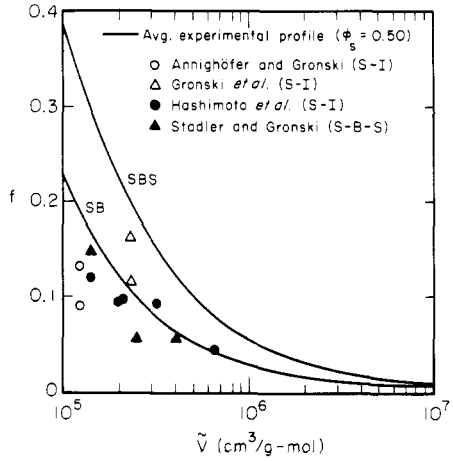

Figure 14. Enlarged section of Figure 13. Data points for styrene–isoprene diblock (SI) copolymers, having spherical and lamellar morphologies, and styrene–butadiene triblock (SBS) copolymers, exhibiting spherical morphology, acquired from SAXS[18,19,31] and DMT[45] measurements are in excellent agreement with the lamellar (ϕ_S = 0.50) SB predictions for f.

$\tilde{V}$ (as was shown earlier for the $\cos^2$ case[14]). The triblock ΔT shows a maximum at $\tilde{V} \approx 90\,000$ cm^3/mol; the diblock exhibits a similar tendency at lower $\tilde{V}$, but the maximum is masked by the onset of homogeneity for $\tilde{V} \leq 25\,000$ cm^3/mol. At $\tilde{V} = 25\,000$ cm^3/mol, the interphase thicknesses between the SB and SBS cases differ by about 20 Å; as $\tilde{V}$ increases, though, this difference decreases to about 1 Å at $\tilde{V} = 10^6$ cm^3/mol.

At $\tilde{V} \approx 10^5$ cm^3/mol, the values of ΔT when $\phi_S = 0.5$ are predicted to be about 40 and 30 Å for the SB and SBS cases, respectively. Hashimoto and co-workers[17,18] report interphase thicknesses for SI block copolymers ranging from 17 to 28 Å at the same molecular weight and similar ϕ_S; their values are comparable to the present predictions, being slightly smaller as expected[14] from chemical differences between isoprene and butadiene that influence δ values (see eq 20). Stadler and Gronski[45] provide evidence that ΔR ranges from 28 to 34 Å for SBS copolymers ($\bar{M}_n$ = 140 000 g/mol) having lower ϕ_S and spherical morphology; this is very close to the present prediction at the higher ϕ_S. At $\tilde{V} \approx 7 \times 10^5$ cm^3/mol the ΔT predictions for the SB and SBS cases in Figure 12 are about 22 and 20 Å, respectively; SAXS investigations[18] report ΔR = 15 Å for SI copolymers with similar $\bar{M}_n$ but lower ϕ_S (spherical morphology). Overall, if we consider that the chemical characteristics of the styrene–butadiene and styrene–isoprene systems are different and the bulk compositions of experimental samples vary somewhat, these comparisons reveal that reasonably good agreement exists between experimental and predicted interphase thicknesses. The data, as well as the predictions (Figure 12 and ref 14), show a $\tilde{V}$-dependence at variance with the narrow-interphase approximation (NIA) developed by Helfand and Wasserman.[10] In addition to this work, some DMT measurements[45] on SBS copolymers having spherical morphology have also demonstrated that the NIA approximation is not valid at low molecular weights ($\bar{M}_n \approx 40\,000$ g/mol).

2. Interphase Fraction. According to SAXS studies,[17-19,31] f decreases with molecular weight. This behavior is successfully predicted in Figure 13, which also shows variations in f from asymmetries in $\phi'_S(x^*)$. At high $\tilde{V}$, the prediction that f becomes vanishingly small is identical to macroscopically phase-separated system behavior, since the two homogeneous phase volumes become dominant.

In the low-$\tilde{V}$ realm, the drastic increase in f signifies the approach of conditions under which the entire sample will be in some kind of mixed state and distinct phase boundaries will not exist. From extrapolating the curves in Figure 13 to $f = 1.0$, we might suspect that microphase separation will not occur in these particular copolymers at 298 K when the molecular weight is less than 18 000–20 000 g/mol. This result, in the case of lamellar SI block copolymers, is in excellent agreement with the SAXS study of Hadziioannou and Skoulios,[46] where transitions from a disordered state to lamellar microstructures were cited at a molecular weight of 20 000 g/mol; fair agreement appears also with their study of SIS copolymers, which gave a transition at about 40000 g/mol.

More detail is presented in Figure 14, where $f(\tilde{V})$ predicted by the model using the experimental $\phi'_S(x^*)$ is shown for the lamellar (ϕ_S = 0.5) morphology in both SB and SBS copolymers. Also shown in Figure 14 are some SAXS and DMT data taken on systems exhibiting spherical and lamellar morphologies. Even though some of these data cannot be directly compared with the model predictions in Figure 14, since they represent SI copolymers, the behavior of these experimentally determined $f(\tilde{V})$ supports the model results by showing identical trends. Excellent agreement is seen between f predicted for the SB copolymer (lamellar morphology) and measured by (a) SAXS for SI copolymers with spherical morphology,[18] where f decreased from 0.21 ($\bar{M}_n$ = 80 000 g/mol) to 0.04 ($\bar{M}_n$ = 657 000 g/mol); (b) SAXS and DMT for SI lamellar morphologies,[19,31] in which f was approximately 0.17 ($\bar{M}_n$ = 230 000 g/mol); and (c) DMT for SBS spherical morphologies,[45] where f decreased from 0.28 ($\bar{M}_n$ = 40 000 g/mol) to 0.03 ($\bar{M}_n$ = 400 000 g/mol).

3. Repeat Distance. The repeat distance, denoted by D in Figure 1, is determined in terms of other microstructural parameters:

spherical/cylindrical domains of styrene

$$D = 2R + T_B - 2\Delta R \tag{23a}$$

lamellar domains

$$D = T_S + T_B - 2\Delta T \tag{23b}$$

Measured values of D, tabulated in Table II for the samples used here, were taken directly from the electron micrographs. In Figure 15, a comparison is made of these $D(\bar{M}_n)$ values with model predictions for the diblock and

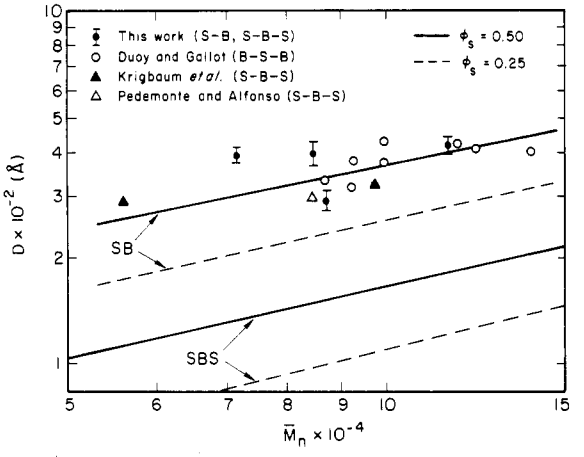

Figure 15. Repeat distances (D) presented as a function of number-average molecular weight. Data in this study (●) have been obtained from electron micrographs exhibiting regions of fully developed structure and agree well with those of other investigators.[47-49] Theoretical predictions are shown for the cylindrical (dashed line) and lamellar (solid line) morphologies, using the average experimental $\phi'_S(x^*)$.

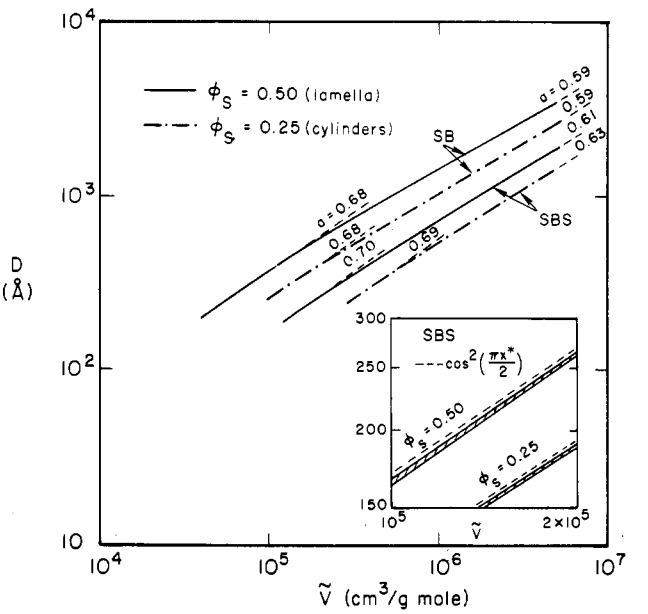

Figure 16. Dependence of repeat distances on molar volume, or approximate molecular weight ($\bar{M}_n$). At the molecular weights of the samples studied ($\tilde{V} \approx 10^5$ cm^3/mol), the slope of each curve is approximately 0.69, which agrees well with 0.67 of other theories.[10-12] At higher molecular weights ($\approx 10^7$ cm^3/mol), this slope decreases to about 0.60. The insert depicts the effect of the experimental profile (shaded) versus the cos^2 profile (dashed) for the range of $\tilde{V}$ corresponding to experimental samples.

triblock copolymers possessing cylindrical (dashed line) and lamellar (solid line) morphologies. Also shown there are similar TEM data from other investigators[47-49] who worked with styrene–butadiene triblock copolymers. The prediction for the diblock lamellar case best fits the entire set of data, which represent cylindrical and lamellar SB, SBS, and BSB copolymers. The reasons for this close agreement of all samples in defining a single $D(\bar{M}_n)$ function are not known, nor is it known why model predictions fail in a general sense (e.g., the SBS predictions lie below the SBS data by a factor of 2.5). It is possible that polydispersity plays a role in the new data reported here, but other data displayed in Figure 15 represent nominally monodisperse samples.

According to the theory proposed by Helfand and Wassermann,[10-12] D for lamellar morphologies should depend on molecular weight as

$$D \propto \bar{M}_n^a \tag{24}$$

where $a \approx 0.67$. Block copolymer samples having spherical, cylindrical, and lamellar morphologies studied by SAXS[17-19] normally have $\bar{M}_n$ on the order of 10^5 g/mol; in this molecular weight regime, $a \approx 0.67$ has been shown to be usually valid for all morphologies. Hadziioannou and Skoulios,[46] however, have reported $a = 0.79 \pm 0.02$ for styrene–isoprene copolymers with $\bar{M}_n < 150\,000$ g/mol and lamellar morphology. Moreover, Henderson and Williams[14] have shown that their theory predicts a should vary approximately from 0.75 at low molecular weights to 0.50 at high molecular weights. Our modification of that theory (using the Debye term and the experimentally determined average $\phi'_S(x^*)$ cited earlier) leads to the predictions shown in Figure 16. There, in the experimental range of $\bar{M}_n$ (1.0–2.3 × 10^5 g/mol), the model predicts $a \approx 0.68$ for cylindrical (dot–dash lines) and lamellar (solid lines) diblocks and $a \approx 0.69$–0.70 for cylindrical and lamellar triblocks, so a determination of a alone is not sufficient to draw distinctions between theories in this regime. The variation in D corresponding to various $\phi'_S(x^*)$, including the experimental band, is seen in the expanded insert. The upper ϕ'_S bound yields the lower limit of the shaded region; that is, an increase in S content within the interphase tends to reduce the magnitude of the repeat distance.

All predictions of $D(\bar{M}_n)$ cited here are for monodisperse polymers. Because experimental evidence exists that polydispersity does have a major impact on the repeat distance,[16,50] care must be taken when claiming support for existing theories when data represent polymers having any polydispersity. Work is currently in progress[51] to develop a theoretical description of $D(\bar{M}_n)$ and other properties in the presence of polydispersity.

4. Free Energy. In view of the common result (in our data and others) that asymmetric $\phi'_S(x^*)$'s arise naturally, it is important to seek an explanation. One hypothesis is that the TEM sample preparation methods (e.g., solvent casting) produce nonequilibrium structures. Another is that the asymmetric case is thermodynamically favored. The latter explanation was examined theoretically by Henderson and Williams[34] for SBS copolymers with lamellar morphologies, their result being that ΔG_{min} decreased as ϕ'_S became richer in styrene (up to a point) for almost all possible $\phi'_S(x^*)$ curve shapes. Also, for a given $\overline{\phi'_S}$, ΔG_{min} was lowest for $\phi'_S(x^*)$ shapes with the least steep slope. The interplay of these factors is complex. The display of $\Delta G_{min}(\overline{\phi'_S}, d)$ by Henderson and Williams[34] in their Figure 5—where d characterizes the profile steepness—can be used to show that a profile with $\overline{\phi'_S} = 0.54$ and $d = 0$ (close to the present data) is favored by about 250 cal/mol over a symmetric profile with sinusoidal shape ($\overline{\phi'_S} = 0.50$, $d = 6$).

We extend the earlier investigation[34] by adding the Debye term to the theory and by examining the cylindrical morphology. As seen in Figure 17, ΔG_{min} from the asymmetric $\phi'_S(x^*)$—measured—is lower than that from the symmetrical cos^2 profile. This is true for both SBS and SB copolymers and at all molecular compositions. The advantage is greatest in the SBS case, the difference being about 1000 cal/mol and representing up to 10% of ΔG_{min}. These results suggest that asymmetric $\phi'_S(x^*)$ are thermodynamically favored in cylindrical morphologies, especially for triblock copolymers. Analogous results exist for the lamellar SB and SBS morphologies,[51] except that ΔG_{min} reductions due to interphase S-enrichment are not as dramatic (i.e., approximately 200 and 400 cal/mol more

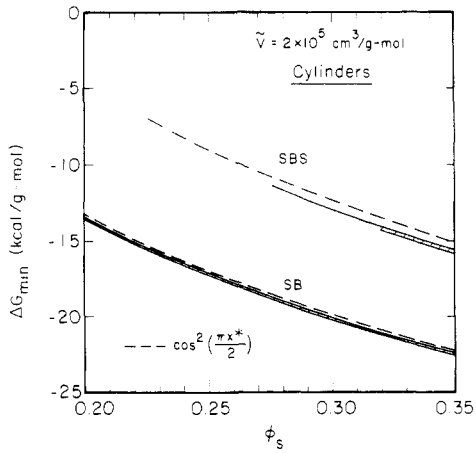

Figure 17. Minimum in Gibbs free energy presented as a function of bulk composition for cylindrical SB/SBS copolymers. The results from the experimental profile (shaded) are seen to be more negative than those from the cos^2 profile (dashed) and are, consequently, favored.

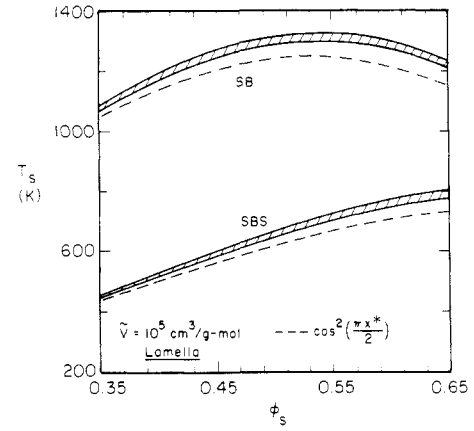

Figure 18. Separation temperature (T_s) for lamellar diblock and triblock cases, predicted as a function of bulk composition by using the experimental profile (shaded) and the cos^2 profile (dashed line).

negative for the SB and SBS cases, respectively).

5. Separation Temperature. An extremely important bulk property is the separation temperature (T_s), the temperature above which microscopic homogeneity is favored. This parameter is calculated by setting ΔG_{min} = 0, determining the values of β_{min}^s and Γ_{min}^s, and then computing $T_s = (\Delta H/\Delta S)_s$. Figure 18 depicts the results of the present theory, for lamellar SB and SBS copolymers, in terms of $T_s(\phi_S)$ at fixed $\tilde{V}$. In the case of the diblock, we see a maximum (1300–1350 K) occurring near ϕ_S = 0.55 and note that the shaded region is 60–80 K higher than the cos^2 profile results. No maximum is observed for the SBS case, within $\phi_S \leq 0.65$, though the $T_s(\phi_S)$ function will yield one[14] at higher ϕ_S (where lamella are not found). This trend for T_s to increase with the content of the hard segment (up to the maximum, anyway) resembles behavior reported by Leung and Koberstein[26] for polyester-based polyurethanes. The SBS case produces less pronounced differences in $T_s(\phi_s)$ for the various $\phi'_S(x^*)$ than does the SB. In both cases, though, T_s increases with increased $\overline{\phi'_S}$ for a fixed ϕ_S.

Conclusions

A method has been presented by which the composition profile across the interphase existing in styrene–butadiene block copolymers has been directly ascertained from transmission electron microscopy. This is apparently the first time $\phi'_S(x^*)$ has been measured directly for block copolymers, with the result that the interphase is found to be rich in styrene (≈54 vol %) for both diblocks and triblocks. This is in excellent agreement with evidence obtained from DMT studies.[28]

Because the measured $\phi'_S(x^*)$'s of the four samples examined are so similar, they are averaged to produce a profile deemed valid for all block copolymers of this type. This profile is then incorporated into the theory developed by Williams and co-workers,[5,6,14,34] along with a modification involving a Debye molecular interaction term. Theoretical predictions of the interphase thickness are of the correct magnitude and correctly show that ΔT and ΔR generally decrease with increasing molecular weight. In addition, the fraction of material in the interphase is predicted (in excellent experimental agreement with the lamellar SB case) to decrease with increasing molecular weight, resembling trends reported for SI[17-19,31] and SBS[45] copolymers. The predicted repeat distance for the lamellar SB case agrees very well with experimental data for SB and SBS copolymers with varying morphologies. The SBS predictions underestimate these distances by a factor of about 2.5. In both cases, the value of a in the expression $D \propto \bar{M}_n^a$ is predicted to be 0.68–0.70 for the data range studied. The separation temperature is predicted to be higher for the experimental profile than for the symmetric profile, corresponding to an increase of T_s with $\overline{\phi'_S}$. Finally, some indication that asymmetric $\phi'_S(x^*)$ can represent a true equilibrium state emerges from the demonstration that the experimental $\phi'_S(x^*)$ is favored over the cos^2 symmetric profile, yielding lower predicted values of ΔG_{min} for both SB and SBS cases.

Acknowledgment. We gratefully acknowledge assistance from D. Kelly of Cosden Chemical and Oil Co. for the block copolymer samples, C. Schooley and the staff of the Electron Microscope Laboratory (University of California, Berkeley) for valuable TEM advice, K. Downing (Lawrence Berkeley Laboratory) and R. Sherwood (Lawrence Livermore National Laboratory) for help in the image-digitizing work, and M. Gelbaum and E. Sheena of the Computer Service Facility (Lawrence Berkeley Laboratory) for consultation. This work was supported by the Director, Office of Energy Research, Office of Basic Energy Sciences, Materials Science Division of the U.S. Department of Energy under Contract DE-AC03-76SF00098.

References and Notes

(1) Diamant, J. Ph.D. Thesis, University of California, Berkeley, 1982.
(2) Henderson, C. P.; Williams, M. C. *J. Polym. Sci., Polym. Lett. Ed.* **1979**, *17*, 257.
(3) Meier, D. J. In *Block and Graft Copolymers*; Burke, J. J., Weiss, V., Eds.; Syracuse University Press: New York, 1973; Chapter 6.
(4) Helfand, E. *Macromolecules* **1975**, *8*, 552.
(5) Leary, D. F.; Williams, M. C. *J. Polym. Sci., Polym. Lett. Ed.* **1970**, *8*, 335.
(6) Leary, D. F.; Williams, M. C. *J. Polym. Sci., Polym. Phys. Ed.* **1973**, *11*, 345.
(7) Krause, S. J. *Macromolecules* **1978**, *11*, 1288.
(8) Meier, D. J. *J. Polym. Sci., Part C* **1969**, *26*, 81.
(9) Krause, S. J. *J. Polym. Sci., Part A-2* **1969**, *7*, 249.
(10) Helfand, E.; Wassermann, Z. R. *Macromolecules* **1976**, *9*, 879.
(11) Helfand, E.; Wassermann, Z. R. *Macromolecules* **1978**, *11*, 960.
(12) Helfand, E.; Wassermann, Z. R. *Macromolecules* **1980**, *13*, 994.
(13) Meier, D. J. *Polym. Prepr. (Am. Chem. Soc., Div. Polym. Chem.)* **1974**, *15* (1), 171.
(14) Henderson, C. P.; Williams, M. C. *J. Polym. Sci., Polym. Phys. Ed.* **1985**, *23*, 1001.
(15) Mayer, R. *Polymer* **1974**, *15*, 137.
(16) Hadziioannou, G.; Skoulios, A. *Macromolecules* **1982**, *15*, 267.
(17) Hashimoto, T.; Shibayama, M.; Kawai, H. *Macromolecules* **1980**, *13*, 1237.

(18) Hashimoto, T.; Fujimura, M.; Kawai, H. *Macromolecules* **1980**, *13*, 1660.
(19) Annighofer, F.; Gronski, W. *Makromol. Chem.* **1984**, *185*, 2213.
(20) Richards, R. W.; Thomason, J. L. *Polymer* **1983**, *24*, 1089.
(21) Richards, R. W.; Thomason, J. L. *Polymer* **1983**, *24*, 275.
(22) Richards, R. W.; Thomason, J. L. *Polymer* **1981**, *22*, 581.
(23) Hadziioannou, G.; Picot, C.; Skoulios, A.; Ionescu, M.; Mathis, A.; Duplessix, R.; Gallot, Y.; Lingelser, J. *Macromolecules* **1982**, *15*, 263.
(24) Richards, R. W.; Thomason, J. L. *Macromolecules* **1983**, *16*, 982.
(25) Bates, F. S.; Dierker, S. B.; Wignall, G. D. *Macromolecules* **1986**, *19*, 1938.
(26) Leung, L. M.; Koberstein, J. T. *Macromolecules* **1986**, *19*, 706.
(27) Hashimoto, T.; Tsukahara, Y.; Tachi, K.; Kawai, H. *Macromolecules* **1983**, *16*, 648.
(28) Kraus, G.; Rollmann, K. W. *J. Polym. Sci., Polym. Phys. Ed.* **1976**, *14*, 1133.
(29) Diamant, J.; Soong, D. S.; Williams, M. C. In *Contemporary Topics in Polymer Science*; Bailey, W. J., Tsurata, T., Eds.; Plenum: New York, 1984; Vol. 4.
(30) Annighofer, F.; Gronski, W. *Colloid Polym. Sci.* **1983**, *261*, 15.
(31) Gronski, W.; Annighofer, F.; Stadler, R. *Makromol. Chem. Suppl.* **1984**, *6*, 141.
(32) Henderson, C. P.; Williams, M. C. *Polymer* **1985**, *26*, 2021.
(33) Wu, S.; Chuang, H.; Han, C. D. *J. Polym. Sci., Polym. Phys. Ed.* **1986**, *24*, 143.
(34) Henderson, C. P.; Williams, M. C. *Polymer* **1985**, *26*, 2026.
(35) Reimer, L. *Transmission Electron Microscopy: Physics of Image Formation and Microanalysis*; Springer-Verlag: New York, 1984; pp 108–109, 185–205.
(36) Spontak, R. J. In *Proceedings of the 44th Annual Meeting of the Electron Microscopy Society of America*; Bailey, G. W., Ed.; San Francisco Press: San Francisco, 1986; p 788.
(37) Spontak, R. J.; Williams, M. C.; Agard, D. A. *Polymer*, in press.
(38) Spontak, R. J.; Williams, M. C.; Schooley, C. N. *J. Mater. Sci.* **1986**, *21*, 3173.
(39) Thomas, H. R.; O'Malley, J. J. *Macromolecules* **1979**, *12*, 323.
(40) O'Malley, J. J.; Thomas, H. R.; Lee, G. M. *Macromolecules* **1979**, *12*, 996.
(41) Russ, J. C.; Russ, J. Ch. In *Microbeam Analysis 1986*; Romig, A. D., Ed.; San Francisco Press: San Francisco, 1986; p 501.
(42) Grum, F.; Becherer, R. J. *Optical Radiation Measurements: Radiometry*; Academic: New York, 1979; p 21–23.
(43) Zielinski, J. M. M.S. Thesis, University of California, Berkeley, 1986.
(44) Meier, D. J. In *Proceedings, Polymer Colloqium*; Kyoto, Japan, Sept 1977.
(45) Stadler, R.; Gronski, W. *Colloid Polym. Sci.* **1982**, *262*, 466.
(46) Hadziioannou, G.; Skoulios, A. *Macromolecules* **1982**, *15*, 258.
(47) Douy, A.; Gallot, B. *Makromol. Chem.* **1972**, *156*, 81.
(48) Pedemonte, E.; Alfonso, G. C. *Macromolecules* **1975**, *8*, 85.
(49) Krigbaum, W. R.; Yazgan, S.; Tolbert, W. R. *J. Polym. Sci., Polym. Phys. Ed.* **1973**, *11*, 511.
(50) Mills, P. J.; Green, P. F.; Palmstrom, C. J.; Mayer, J. W.; Kramer, E. J. *J. Polym. Sci., Polym. Phys. Ed.* **1986**, *24*, 1.
(51) Spontak, R. J., unpublished calculations for Ph.D. in progress, University of California, Berkeley, 1986.

Cylindrical Micelles Formed by a Charged Comb-Shaped Copolymer in Aqueous Solutions Studied by Small-Angle Neutron Scattering

L. B. Shih,*† E. Y. Sheu,‡ and S. H. Chen§

Polymer Research Department, S. C. Johnson & Son, Inc., Racine, Wisconsin 53403, and Department of Nuclear Engineering, Massachusetts Institute of Technology, Cambridge, Massachusetts 02139. *Received July 6, 1987; Revised Manuscript Received October 23, 1987*

ABSTRACT: We present the analysis of a series of small-angle neutron scattering data of a comb-shaped copolymer, poly(1-octadecene-*co*-(maleic anhydride)), dissolved at various concentrations in D_2O at room temperature. The results show at full ionization the copolymers self-associate to form cylindrical micelles with a radius of 27 Å and a length of 99 Å. At low concentrations, the number of repeating units of the copolymer per micelle is determined to be 233 ± 5 and the hydration number per hydrophilic head group equals 10. The number of repeating units gradually decreases to 98 with concomitant increase in the hydration number to 30 at 20 wt % solution. This indicates that the system tends to lower its free energy by decreasing the aggregation number of micelles at higher concentrations.

I. Introduction

Synthetic polyelectrolytes in aqueous solutions have been the focus of many studies.[1-3] These polymers are important in many industrial applications because the conformational states of these polymers in solution often influence the solution behavior, such as the rheological property. Especially interesting are some polyelectrolytes with amphiphilic characteristics; they exhibit waxy properties and yet are soluble in water.

Our main interest in this work is the aggregational behavior of a comb-shaped alternating copolymer poly(1-octadecene-*co*-(maleic anhydride)), abbreviated as PODMA, in water. The copolymers form clear solutions at moderate concentrations when the diacid groups are fully neutralized with the hydroxides of alkaline metal ions. The molecular structure of one repeating unit in the diacid form is depicted in Figure 1. Earlier studies with a similar class of copolymer, (alkyl vinyl ether)-*co*-(maleic anhydride), by Dubin and Strauss[2-5] using potentiometric titrations and viscosity measurements have shown that the conformational states of these polymers are strongly influenced by the degree of ionization of the diacid head group. Their studies were centered around copolymers with shorter side chains in comparison to PODMA. They proposed that the copolymers form hypercoiled "intramolecular" micelles. However, our recent solubilization measurements of PODMA using Raman and FTIR[6] have clearly shown the partition of benzyl alcohol in the hydrocarbon and aqueous phases. The results are indicative of the formation of hydrocarbon domains in water.

Carbon-13 NMR measurements[7] of PODMA solutions have shown that the chemical shifts of the side-chain methylene groups (C_5–C_{14}) are unchanged in solutions with concentrations ranging from 50 to 2000 ppm. Similar measurements with sodium alkylsulfates and other surfactants[8,9] have demonstrated that the chemical shift

† S. C. Johnson & Son, Inc.
‡ Massachusetts Institute of Technology. Present address: Exxon Research & Engineering Co., Clinton Township, Annandale, NJ 08801.
§ Massachusetts Institute of Technology.

0024-9297/88/2221-1387$01.50/0 © 1988 American Chemical Society